Available online at www.sciencedirect.com
SCIENCE DIRECT®
ELSEVIER
International Journal of Multiphase Flow 31 (2005) 739–756
International Journal of Multiphase Flow
www.elsevier.com/locate/ijmulflow

A computational analysis of the hydrodynamic instability of a liquid jet focused into a converging microchannel

S. Hardt [a,*], F. Jiang [b], F. Schönfeld [b]

[a] *Chair of Technical Thermodynamics, Darmstadt University of Technology, Petersenstrasse 30, D-64287 Darmstadt, Germany*
[b] *Institute of Microtechnology Mainz, Carl-Zeiss-Str. 18-20, D-55129 Mainz, Germany*

Received 8 April 2004; received in revised form 12 January 2005

Abstract

The instability of a focused liquid jet is studied by semi-analytical methods and by methods of computational fluid dynamics. The semi-analytical approach relies on earlier work on the instability of an extending liquid thread and is based on the Stokes flow regime and small-amplitude perturbations. The evolution of different excitation modes is evaluated and compared. Through hydrodynamic focusing and the corresponding extensional flow an initially stable mode may become unstable and it depends on the position away from the inlet which mode is to be regarded as the most unstable one. When plotting a hypothetical jet decay length against the excitation wave number, a comparatively broad minimum is exhibited. The CFD simulations based on the volume-of-fluid method show that the jet may break up either in the conical focusing zone or in the attached capillary, depending on the flow velocity. When the deformation of the jet surface reaches a certain amplitude, the jet assumes a ''beads-on-a-string'' structure instead of a shape derived from a harmonic perturbation. A jet decay within the capillary produces elongated droplets with cusped ends. When comparing the results of the CFD and the semi-analytical model, it turns out that the CFD simulations predict more stable jets with a larger decay length. An analysis of the flow velocity field shows that the increased stability might be due to the interaction of the jet with the channel walls.
© 2005 Elsevier Ltd. All rights reserved.

* Corresponding author. Tel.: +49 6151 163159; fax: +49 6151 166561.
E-mail address: hardt@ttd-tu-darmstadt.de (S. Hardt).

0301-9322/$ - see front matter © 2005 Elsevier Ltd. All rights reserved.
doi:10.1016/j.ijmultiphaseflow.2005.01.006

Keywords: Hydrodynamic instabilities; Hydrodynamic focusing; Liquid jet; Computational fluid dynamics; Free surface flow

1. Introduction

The decay of liquid jets into droplets is a phenomenon which has found widespread applications in various technological areas. Perhaps the most well known and economically relevant application relates to ink-jet printers which produce droplets via the decay of an ejected liquid jet (see, e.g., Yeh, 2001). Droplet formation from a jet also occurs in electrospray ionization mass spectrometers, in which the droplets are generated owing to the instability of an ionic liquid surface in strong electric fields (for an overview, see Cole, 1997). For the development of the electrospray technology the 2002 Nobel Prize in chemistry was issued to John B. Fenn. Another highly relevant application is flow cytometry. In flow cytometers cells carried by a fluid stream are analyzed in flow and specific cells may be separated from the stream in order to allow for a more detailed morphological or biochemical analysis. This separation and sorting of cells may occur via a thin liquid thread which decays into droplets each containing a single cell (Ormerod, 1999). The electrically charged droplets can then be deflected in an electrostatic field.

The diameter of a liquid jet is usually given via the diameter of the nozzle from which the jet emerges. This induces a direct relationship between the nozzle diameter and the size of the droplets created from the jet. In order to increase the flexibility of the process and to allow generation of droplets smaller than the nozzle diameter, it has been proposed to focus a jet hydrodynamically: By hydrodynamic shear forces exerted on the liquid surface via a surrounding fluid the jet diameter is continuously decreased. One method to achieve hydrodynamic focusing is to force the jet and the surrounding fluid through a narrow constriction. This principle was demonstrated by Gañán-Calvo (1998) using a liquid jet in the core of a highly accelerating gas stream. He was able to create monodisperse sprays with a droplet diameter below 100 μm from an orifice of 800 μm diameter.

In recent years, the processing and control of fluids in microreactors, micrototal analysis systems (μTAS) and other microfluidic devices has experienced a rapid development. The prerequisite for this development was the progress in microfabrication technology, allowing to create MEMS devices with a broad variety of geometries and designs. In the beginning, mainly systems for single-phase microflows were studied. Recently, an increasing number of publications on two-phase flows have appeared. Especially for free-surface flows microsystems offer a degree of control unparalleled by macroscopic devices, as due to the large surface-to-volume ratio the dynamics of the three-phase contact line at the channel walls has a major influence on the flow patterns. In this context, gas/liquid (Kawahara et al., 2002; Akbar et al., 2003; Hetsroni et al., 2003) as well as liquid/liquid systems (Haverkamp et al., 1999; Hardt et al., 2001; Sugiura et al., 2001; Thorsen et al., 2001; Dreyfus et al., 2003; Anna et al., 2003) have been studied. Anna et al. (2003) have begun to investigate hydrodynamic focusing in oil/water microfluidic systems and were able to show that the size distribution of oil droplets in water can be tuned over a wide range when varying the liquid flow rates. Such a control over two-phase flows offers interesting perspectives for the creation of tailor-made microemulsions or suspensions of micro- or nanoparticles. An application of two-phase microfluidic systems which has already been established is the generation of microcapsules for drug delivery

(Freitas et al., 2003). In this case, a solvent extraction method is utilized to create particles from a microemulsion which may serve as drug carriers in the human body.

For applications such as the generation of emulsions or particles throughput is an issue, i.e., it is desirable to produce a large enough product quantity per unit time. At the Institute of Microtechnology Mainz micromixers have been developed which allow to create a multitude of parallel liquid lamellae or jets decaying into droplets, thus enabling a higher throughput than the common systems which usually bring together only a few streams of immiscible fluids. For better visualization of the flow patterns such multilamination mixers were fabricated by mikroglas technik AG, Mainz, Germany, from photostructurable glass based on a UV-lithography process. Through a multitude of interdigitated inlets the fluids enter into a mixing zone of 3 mm width and 150 μm depth, as displayed in Fig. 1. The inlets of 60 μm width are separated by partition walls of 50 μm width. Besides the mixing zone, the mixer comprises a flow distribution manifold allowing to distribute the fluids equally over the different inlets. The system is assembled from a number of microstructured layers which are thermally bonded together. Fig. 1 demonstrates that hydrodynamic focusing may be employed to influence and tune the size distribution of the droplets created. In the corresponding experiments (Pennemann et al., 2004) dyed water (black) and silicon oil (white, Silicon Oil DC 200, Fluka) were used, the ratio of flow rates was fixed to 1:10 (silicon oil:water) and the total flow rate was varied. At the interdigitated inlets, the water velocity exceeds the silicon-oil velocity by a factor of 10. Further downstream, as a result of shear forces, the velocities of the two liquids adapt, causing a decrease of the water and an increase of the silicon-oil velocity. Correspondingly, owing to the incompressibility of the two liquids, the cross section of the silicon-oil jets decreases, thus resulting in a hydrodynamic focusing similar as observed by Anna et al. (2003). By adjusting the total flow rate at a fixed flow rate ratio, either large (small total flow rate) or small droplets (high total flow rate) are created.

These examples demonstrate the far reaching capabilities of microfluidic systems for processing of two-phase flows and especially the potential of hydrodynamic focusing. In order to allow a more efficient design of such systems, it is necessary to better understand the fluid dynamics and the mechanisms of droplet formation. The pioneering theoretical work on the formation of droplets from a liquid jet, or more precisely, a liquid rod (as the system was considered to be at rest) was done by Rayleigh and Plateau already in the 19th century (see, e.g., Eggers, 1997).

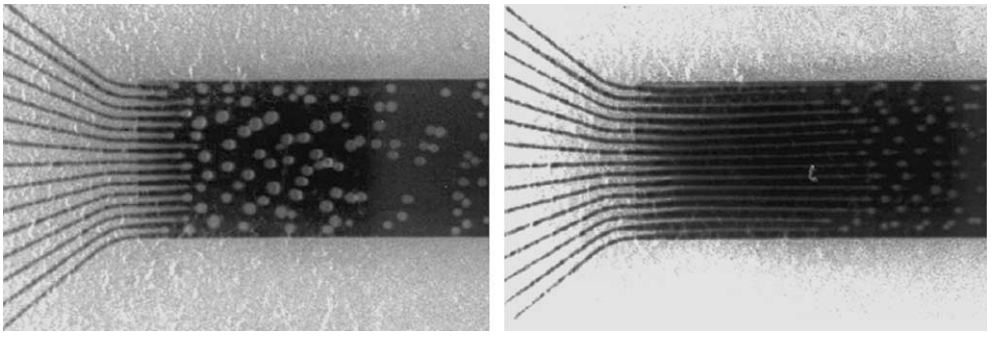

Fig. 1. Formation of a silicon-oil-in-water emulsion in an interdigital micromixer at a flow rate ratio of 1:10 (Pennemann et al., 2004). On the left side, droplet formation occurs close to the inlets (total flow rate: 880 ml/h) whereas on the right side at a total flow rate of 1760 ml/h extended jets of silicon oil are created.

They considered sinusoidal small-amplitude perturbations of the circumference of the rod and solved the hydrodynamic equations in the limit of inviscid irrotational flow. On this basis they were in some cases able to predict the size of the droplets created from the rod which is determined by the wavelength of the fastest growing mode of a hydrodynamic instability. Since then the comparatively simple Rayleigh-Plateau linear stability theory was extended to a number of more realistic scenarios. One of the most important contributions in this context is due to Chandrasekhar (1961) who considered the full Navier–Stokes scenario in the limit of small perturbations.

To the knowledge of the authors, the stability of a hydrodynamically focused liquid jet has so far not been investigated. The present article serves the purpose to study this problem in an approximate manner in order to provide some guidelines for the design of specific microfluidic systems. For the sake of simplicity, the Stokes flow regime is considered. In the first part of the paper, the growth of perturbations on a focused liquid jet is computed analytically in the framework of linear stability theory. Subsequently, methods of computational fluid dynamics (CFD) are employed in the second part of the paper to study large deformations of the liquid interface and especially the decay into droplets. The corresponding CFD simulations are based on a surface-capturing technique and have to be regarded as complementary to the analytical calculations.

2. Stability analysis of a focused jet in the Stokes flow regime

The situation to be considered in the following is depicted in Fig. 2. A liquid jet is focused into a conical channel oriented along the z-direction. The jet has a local radius $a(z)$ and is surrounded by a second immiscible liquid. Axial symmetry is assumed. In cases where $|\mathrm{d}a/\mathrm{d}z| \ll 1$, a local observer co-moving with the jet would experience a situation as shown on the right side of Fig. 2: The diameter of the jet decreases as a function of time owing to a radial inflow being redirected to an outflow in positive and negative z-direction. For the forthcoming stability analysis the following assumptions are made:

1. The flow occurs at sufficiently small Reynolds numbers such that the Stokes flow regime applies.
2. The focusing of the jet occurs slowly enough, i.e., $|\mathrm{d}a/\mathrm{d}z| \ll 1$ and $\lambda \ll a|\mathrm{d}z/\mathrm{d}a|$, where λ is the wavelength of the perturbation.

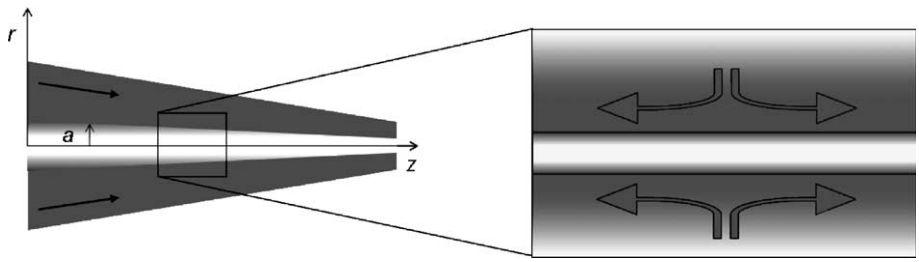

Fig. 2. On the left side, a liquid jet (light gray) focused into a conical channel and surrounded by a second immiscible liquid (dark gray) is displayed. The right side shows the local flow profile as seen from an observer co-moving with the jet.

3. The perturbations applied to the surface of the jet are axially symmetric, sinusoidal and of sufficiently small amplitude such that only terms linear in the excitation amplitude need to be retained.
4. The influence of the walls of the conical channel shown in Fig. 2 on the jet is neglected, i.e., the parabolic flow profile is replaced by a flat profile in the vicinity of the jet.

Among these, the key assumption for the analysis presented in this section is no. 3. For a co-moving observer, the jet appears as a liquid thread suspended in an extensional flow. In the co-moving frame-of-reference the components of this extensional flow are given by

$$u_r = -\frac{1}{2}Gr, \quad u_\phi = 0, \quad u_z = Gz, \tag{1}$$

where G is the extension rate and cylindrical coordinates (r, ϕ, z) are used. In general G is a function of time and depends on the geometry of the focusing zone. For the following stability analysis, the focusing zone does not necessarily have to be a channel of conical shape, but more general geometries with channel walls following an arbitrary envelope are allowed as long as the condition no. (2) is fulfilled. In order to study the stability of the jet, a small perturbation of its radius with wave number k is assumed

$$a \rightarrow a + \alpha_0 \cos kz. \tag{2}$$

The perturbation is imposed onto the jet at $t = 0$ and convected downstream into the channel. For the further analysis it is assumed that the origin of the perturbation is at $z = 0$ which could be the position of an orifice from which the jet emerges. The physical reason for the perturbation could be, e.g., pressure fluctuations in the feed line. In general it can be difficult to identify the exact origin of the perturbations inducing the decay of a jet. Assuming perturbations being imposed at $z = 0$ can be questionable in some cases. However, while some uncertainty with regard to the general validity persists, this model assumption at least describes the cases where perturbations are induced deliberately by an actuator coupled to the orifice. An example of such a scenario is a vibrating orifice used to control jet decay (see, e.g., Brenn and Lackermeier, 1997).

The fate of the liquid jet now depends on the time-evolution of the perturbation modes in the co-moving frame of reference. Mikami et al. (1975) studied the stability problem of an extending liquid thread up to linear order in the perturbation amplitude quite a while ago. With the flow field of Eq. (1) they found an expression of the perturbation amplitude as a function of time of the form

$$\frac{\alpha(t)}{\alpha_0} = \left(\frac{x(t)}{x_0}\right)^{1/3} \exp \int_0^t \left[\frac{\gamma}{2\eta a_0}\left(\frac{x_0}{x}\right)^{1/3}(1-x^2)\Phi(x) - \frac{3}{2}G\left(\frac{\eta^*}{\eta}-1\right)\overline{\Phi}(x)\right] \mathrm{d}t. \tag{3}$$

The subscript "0" refers to the value of a quantity at $t = 0$ in each case. The material parameters entering this expression are the dynamic viscosity of the outer liquid η, the dynamic viscosity of the inner liquid η^*, and the interfacial tension γ. The time evolution of x, the product of the jet radius a and the perturbation wave number k is given by

$$\frac{x(t)}{x_0} = \exp\left[-\frac{3}{2}\int_0^t G\,\mathrm{d}t\right]. \tag{4}$$

The symbols Φ and $\overline{\Phi}$ in Eq. (3) represent quite complicated functionals of modified Bessel functions and can be looked up in the original work of Mikami et al. In order to determine the perturbation amplitude at a specific value of z, the time integral in Eq. (3) is replaced by a space integral via

$$\int_0^t \mathrm{d}t = \int_0^{z(t)} \frac{\mathrm{d}z}{u_{\mathrm{jet}}}, \tag{5}$$

where u_{jet} is the average velocity of the liquid jet. For computation of the spatial evolution of the perturbation amplitude, the extension rate G which depends on the specific geometry of the focusing zone needs to be determined. By using the flow field of Eq. (1) it is easy to show that the jet radius evolves as

$$a(t) = a_0 \exp\left[-\frac{1}{2}\int_0^t G\,\mathrm{d}t\right]. \tag{6}$$

In a given geometry of the focusing zone a jet of a certain shape $a(t) = a(z(t))$ develops, where the transformation between space and time is done according to Eq. (5). The functional form of the extension rate G can then be derived from Eq. (6). When inserting this function into Eq. (3) and relating space and time coordinates via the average jet velocity, the perturbation amplitude $a(z)$ can be determined.

Under different flow conditions, focused jets of various shapes may be formed. In general it is necessary to solve the Stokes equation together with the appropriate boundary conditions for the normal and tangential stresses on the interface between the two liquids to determine $a(z)$. The example to be considered here is a jet focused into a conical channel, with the corresponding geometry sketched in Fig. 3. For simplicity the inner and the outer liquid are assumed to have the same dynamic viscosity, i.e., $\eta = \eta^*$. To further simplify the calculation, a focusing zone with a length L large compared to its radius R is considered. In that case lubrication theory, dating back to the original work of Reynolds (1886), can be applied to compute the flow field. Lubrication theory is based on an expansion of the Navier–Stokes equation in the ratio of the length scales in flow direction and perpendicular to the flow, i.e., R/L. For the axisymmetric geometry of Fig. 3 and to leading order in R/L, the following equations are obtained for the pressure p and the longitudinal and transversal velocity components:

$$\frac{\eta}{r^2}\frac{\partial}{\partial r}\left(r^2\frac{\partial u_z}{\partial r}\right) = \frac{\partial p}{\partial z}, \tag{7a}$$

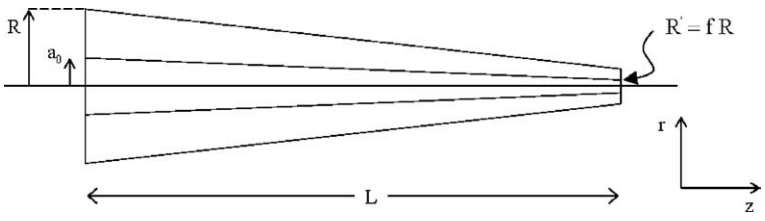

Fig. 3. Model geometry of a conical channel for focusing of a liquid jet. At the inlet the jet and the channel have a radius of a_0 and R, respectively. After a length L the channel diameter is decreased to $f \cdot R$, with $f < 1$.

$$u_r = 0, \tag{7b}$$

$$\frac{\partial p}{\partial r} = 0. \tag{7c}$$

From these expressions it immediately follows that locally the flow is described by a Poiseuille profile in every part of the domain. When globally adjusting the streamlines to follow the channel walls at the domain boundary, the jet diameter is decreased by the same amount as the channel diameter

$$a(z) = a_0 + (f-1)\frac{z}{L}a_0. \tag{8}$$

The z-dependence of the mean flow velocity $\bar{u}$ inside the channel can be obtained from the law of mass conservation which states that $\bar{u}(z)A(z) = \text{constant}$, where $A(z)$ is the cross-sectional area at position z. Hence,

$$\bar{u}(z) = \frac{\bar{u}_0}{\left(1 + (f-1)\frac{z}{L}\right)^2}. \tag{9}$$

The velocity profile is then obtained as

$$u_z(r,z) = \frac{2\bar{u}(z)}{R^2\left(1 + (f-1)\frac{z}{L}\right)^2}\left(R^2\left(1 + (f-1)\frac{z}{L}\right)^2 - r^2\right). \tag{10}$$

In this analysis up to now the two-phase nature of the flow has been ignored. At the interface between the two liquids, the stress tensor T_{ij} has to fulfill the boundary condition

$$\sum_j T_{ij}n_j\Big|_{\text{in}} = -\frac{\gamma}{a}n_i + \sum_j T_{ij}n_j\Big|_{\text{out}}, \tag{11}$$

where the subscripts "in" and "out" indicate the inner and the outer liquid, respectively, and n_i denote the components of an outward normal vector. In the framework of the lubrication approximation used here this boundary condition can be fulfilled by setting

$$p(z)|_{\text{in}} = p(z)|_{\text{out}} + \frac{\gamma}{a}. \tag{12}$$

As the jet radius a depends on z, the pressure distribution inside the jet differs from the pressure distribution outside. Owing to the counter pressure from surface tension, the jet velocity decreases compared to the description given in Eq. (10), i.e., a correction is added to the Poiseuille profile. However, one should keep in mind that in the limit considered here ($|\mathrm{d}a/\mathrm{d}z| \ll 1$, $R/L \ll 1$) the main pressure drop is due to viscous dissipation and not to changes in the interfacial curvature. For this reason, these higher-order corrections to the Poiseuille profile are discarded here. The CFD simulations presented in the next chapter show that this is a reasonable approximation and that the shape of the jet is described by Eq. (8) with sufficient accuracy, apart from perturbations of its surface due to hydrodynamic instabilities.

The average jet velocity, required for the transformation between space and time coordinates, is determined from

$$u_{\mathrm{jet}}(z) = \frac{\int_0^{a(z)} u_z(r,z) r \,\mathrm{d}r}{\int_0^{a(z)} r \,\mathrm{d}r}. \tag{13}$$

Hence, while the influence of the Poiseuille flow profile is neglected as long as the hydrodynamic instability is concerned, it is accounted for when computing the average jet velocity. Using $\mathrm{d}z/\mathrm{d}t = u_{\mathrm{jet}}$ it is straightforward to derive the relationship between the spatial and temporal coordinates of an observer co-moving with the jet

$$t = \frac{z + (f-1)\frac{z^2}{L} + (f-1)^2 \frac{z^3}{3L^2}}{2\bar{u}_0\left(1 - \frac{a_0^2}{2R^2}\right)}. \tag{14}$$

From Eq. (6) the extension rate G can be determined. However, in the case considered here ($\eta = \eta^*$), the second term in the integrand of Eq. (3) vanishes and G does not need to be determined explicitly. From Eqs. (4) and (6) one obtains the relationship

$$x(t) = x_0 \left(\frac{a(t)}{a_0}\right)^3. \tag{15}$$

From that and with the use of Eqs. (8) and (14), the integral in Eq. (3) can be computed after transformation to spatial coordinates, yielding the perturbation amplitude as a function of z. The corresponding equation is given as

$$\frac{\alpha(z)}{a(z)} = \frac{\alpha_0}{a_0} \exp\left[\frac{\gamma L}{2\eta a_0 \bar{u}_0} \int_0^{z/L} \left(\frac{x}{x_0}\right)^{1/3} (1-x^2)\Phi(x) \frac{\mathrm{d}\tilde{z}}{\tilde{u}}\right], \tag{16}$$

where a dimensionless coordinate $\tilde{z} = z/L$ and a dimensionless velocity $\tilde{u} = u/\bar{u}_0$ have been introduced. From this expression it is obvious that there are three dimensionless parameters determining the relative strength of the perturbation with respect to the mean diameter of the jet $a(z)$: (1) the relative perturbation amplitude at the inlet α_0/a_0; (2) the dimensionless group $\kappa = \gamma L/(2\eta a_0 \bar{u}_0)$; (3) the dimensionless perturbation wave number at the inlet x_0. The dependence on the first two of these parameters is more or less trivial, as they effect a scaling of the perturbation amplitude and a scaling of the integral.

For the following studies, the geometry parameters of the flow domain were chosen as $R = 20$ μm, $L = 1000$ μm, $f = 0.1$. Hence, the conditions $|\mathrm{d}a/\mathrm{d}z| \ll 1$ and $R/L \ll 1$ are clearly fulfilled. The liquid properties used were $\eta = \eta^* = 0.1$ Pa s, $\gamma = 10^{-2}$ N/m and the parameters determining the inlet conditions were set to $a_0 = 5$ μm, $\bar{u}_0 = 0.1$ m/s, if not stated otherwise. The reason why the single values rather than the dimensionless groups are given explicitly here is the fact that the same parameters were used for the CFD simulations presented in the following section. With a typical liquid density of 1000 kg/m^3 a Reynolds number of 5×10^{-3} is obtained, thus justifying the use of the creeping flow approximation. While the effect of variations of α_0/a_0 and κ is easy to predict, the main focus of the numerical studies was to follow the growth of the perturbations for different values of x_0. The evaluation of the integral appearing in Eq. (16) was done numerically using Simpson's rule. Corresponding results are displayed in Fig. 4. Apparently there is a qualitative change in the dynamical behavior when x_0 is varied. For relatively large values of the dimensionless perturbation wave number the perturbation is damped initially. For $x_0 \leqslant 2\pi/7$

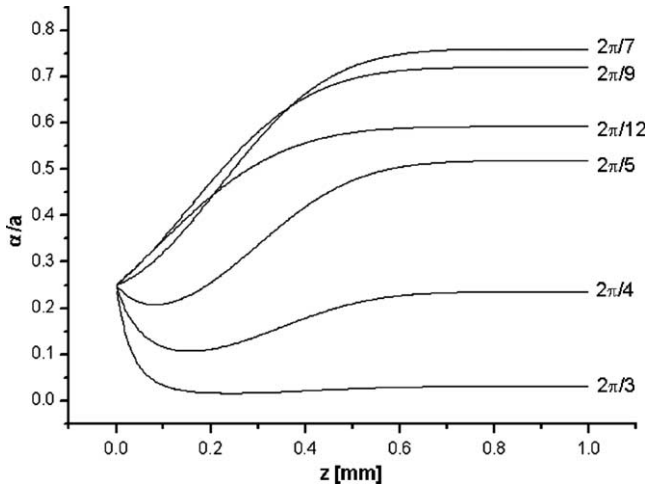

Fig. 4. Evolution of the relative perturbation amplitude over a focusing zone of 1 mm length for various values of x_0.

such a damping is no longer observed. The origin for this effect lies in the wavelength scaling due to hydrodynamic focusing. It is well known that the local condition for instability of a liquid jet is $x(z) < 1$ (see, e.g., Chandrasekhar, 1961). For dimensionless wave numbers larger than 1 the perturbation amplitude decreases initially until x falls below 1 due to the extensional flow and the scaling described in Eq. (4). From that point on, the perturbation increases. As apparent from the figure, the smallest value of x is not related to the fastest growing perturbation. Already Rayleigh in his pioneering work on liquid jet decay was able to show that there is a mode of maximum instability. In the case considered here, both the jet diameter and the perturbation wave number are a function of z. For this reason the growth rate of the perturbations changes in streamwise direction and at different z positions the fastest growing perturbation is caused by different excitation modes at the inlet, as apparent from the crossing of some of the curves. Close to the exit of the focusing zone the velocity of the jet increases rapidly, causing a flattening of the curves of Fig. 4 due to the decrease of residence time. It is worth while to note that when the focusing ratio f goes to zero, the flow velocity at the exit of the focusing zone goes to infinity.

In experiments with focused liquid jets the most pronounced feature to detect is the decay of the jet into droplets. The linear stability theory employed here to predict the time evolution of perturbations is unable to describe the final stages of the droplet formation, as for large perturbation amplitudes a linearization of the equation of motion for the liquid interface is no longer allowed. Being aware of these shortcomings we naively define a decay length z_d by the condition

$$z_d = z|_{\alpha=a}. \tag{17}$$

The purpose of this definition is to provide an order-of-magnitude estimate for the length the liquid jet attains before decaying into droplets. In Fig. 5 the relative decay length is plotted as a function of $2\pi/x_0$ for $\alpha_0/a_0 = 0.25$ and different values of the dimensionless parameter κ. Apparently, for each value of κ there is a mode with maximum growth rate leading to a minimal value of z_d/L. For increasing κ the value of x_0 related to the minimum of the curve decreases and the minimum becomes very shallow. It is thus expected—at least in the framework of linear stability

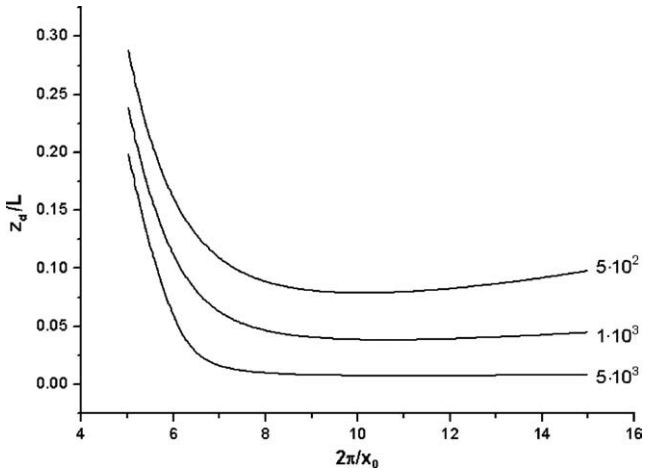

Fig. 5. Relative decay length z_d/L as a function of $2\pi/x_0$. The different curves are labeled with the dimensionless parameter κ.

theory—that in cases where a spectrum of perturbations is imposed on the jet, the breakup into droplets cannot always uniquely be assigned to the most unstable mode and slightly different distributions of the spectral power might lead to different decay modes.

3. CFD simulations

The semi-analytical model presented in the previous section has the advantage of making the dependence of the flow field on the governing dimensionless groups transparent and allows a rapid numerical evaluation. However, its range of applicability is limited. Besides the restriction to small-amplitude perturbations and to slowly focused jets the creeping flow approximation used is limited to small Reynolds number flows. Furthermore rotational symmetry was assumed, while in practice more complex geometries might be encountered. For studying more general scenarios a semi-analytical approach is no longer practicable and it is necessary to employ CFD methods.

Among the CFD algorithms used for the problem under study, the quality of the numerical results usually depends strongly on the method for computing the evolution of the fluid interface. Here, the volume-of-fluid (VOF) method is employed for the free-surface flow problem (for an overview, see Ferziger and Perić, 2002). In the framework of the VOF method a volume-fraction function f is introduced which assumes a value of either 0 or 1, depending on which fluid phase a computational cell belongs to. The volume-fraction function then obeys a convection equation of the form

$$\frac{\partial f}{\partial t} + \sum_i u_i \frac{\partial f}{\partial x_i} = 0, \tag{18}$$

where u_i are the components of the flow velocity. In addition to that, the incompressible Navier–Stokes equation and the equation of mass conservation are solved. In order to account for

different physical properties of the two fluid phases, the viscosity and density have to be regarded as a function of f.

All simulations reported here were performed with the commercial flow solver CFX4 (CFX/Ansys) based on the finite-volume method. For the implementation of surface tension the approach of Brackbill et al. (1992) was used. For discretization of the convective term in the Navier–Stokes equation the Upwind scheme and in the volume-fraction equation the QUICK scheme (Leonard, 1979) was chosen. The SIMPLEC algorithm (Van Doormal and Raithby, 1984) was used as pressure-correction scheme. The numerical solution of Eq. (18) based on a low-order differencing scheme often suffers from errors known as numerical diffusion. Owing to these errors the fluid interface becomes blurred and after a number of time steps it may happen that a sufficiently accurate interface reconstruction becomes impossible. Within CFX4 a so-called surface-sharpening algorithm is used to prevent blurring of the interface. This algorithm records the amount of fluid of a specific phase having passed the interface at each time step and redistributes the fluid as to compensate for numerical diffusion. The redistribution is done in such a way that the computational cells for which initially $f = 1$ are refilled with fluid to an equal percentage α, i.e., $f_{\text{new}} = f_{\text{old}} + \alpha(1 - f_{\text{old}})$, and that mass is conserved independently for both phases.

When working with such a rather artificial correction algorithm it is important to check whether it produces meaningful results when studying free-surface flows in general and hydrodynamic instabilities in particular. For validation purposes the results of the VOF model described above were compared to earlier work on jet breakup based on a moving-grid finite-element method (Ashgriz and Mashayek, 1995). In the latter method the computational grid is updated such as to accommodate the shape of the deforming jet, i.e., surface tracking is performed. In contrast, the VOF approach belongs to the class of surface capturing methods and is based on a fixed grid. In the method of Ashgriz and Mashayek there is no outer fluid. Correspondingly the only contribution to the stress tensor on the free surface is the Laplace pressure due to surface curvature. The VOF approach, however, accounts for the flow fields of both the inner and the outer fluid. For this reason the equations become increasingly stiff if the material properties (density, viscosity) differ by a large amount and numerical instabilities usually occur. In order to avoid convergence problems while still suppressing the influence of shear forces exerted by the outer fluid, its viscosity was set to 10^{-3} of that of the inner fluid. The simulations were then performed with an initial configuration which consists of a sinusoidal perturbation superposed on a cylindrical jet. Ashgriz and Mashayek used a perturbation amplitude of 5% of the unperturbed jet radius. Since the VOF method is less capable of resolving fine deformations of a fluid interface than the moving-grid technique, a larger relative perturbation of 15% was used here.

The result of the comparison between the surface-tracking and the surface-capturing method is displayed in Fig. 6. Both simulations were performed for a Reynolds number of 0.1 (corresponding to the low-Reynolds number regime studied in this paper) and a perturbation wavelength of 31.4 times the jet radius. The Reynolds number is defined based on the properties of the inner fluid and given as $Re = (1/\nu)(\gamma a_0/\rho)^{1/2}$ where a_0 is the initial jet radius and ν, ρ are kinematic viscosity and density, respectively. The different frames are labeled by a dimensionless time parameter obtained by dividing the actual time by the characteristic time scale $(\rho a_0^3/\gamma)^{1/2}$. Time zero corresponds to the instance of jet breakup. By construction, the moving-grid technique of Ashgriz and Mashayek is unable to predict the breakup point. Owing to this fact they assumed that the jet breaks up after the radius has been reduced to 1% of its initial value. When comparing the

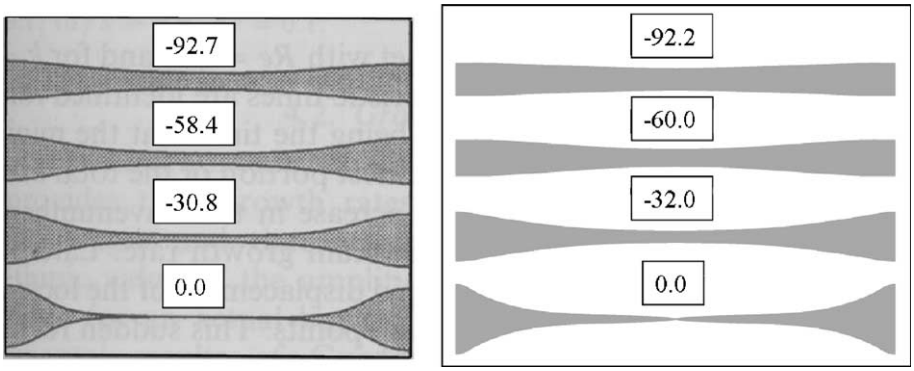

Fig. 6. Time evolution of a viscous jet as obtained from the moving-mesh (left) and the VOF method (right). The figure shows a section along the jet corresponding to half the excitation wavelength.

results of the two different methods it becomes apparent that the VOF method predicts an earlier decay than the moving-grid technique. Despite this fact the dynamical evolution of the jet is very similar in both cases. The accelerated jet breakup predicted by the VOF method might be due to the reduced number of computational cells available to resolve the velocity field in an increasingly thinner jet. In Fig. 6 the radial extension of the jet is resolved with five cells close before breakup. The reduced number of computational cells in such a case is inherent to a surface-tracking method such as VOF and usually leads to a loss of numerical accuracy. In order to model the jet dynamics close to breakup more accurately techniques such as described by Eggers (1997) would be more appropriate. However, the scope of this paper is to give an overview of the dynamics rather than studying specific details with high accuracy. For the same reason we have settled for comparing the VOF results qualitatively with the results of Ashgriz and Mashayek. A more quantitative comparison with, e.g., the spatial instability of a viscous jet for which Lin and Lian (1990) have derived an analytical formula would have been quite difficult and requires considerable computational resources, since the analytical results are based on an inviscid ambient fluid, a situation which leads to numerical instabilities, as mentioned above.

For the computational domain corresponding to a jet focused into a converging channel an axially symmetric geometry model with a focusing zone as described in the previous section was set up. In order to be able to follow the further development of the jet, a capillary section of 300 μm length was attached to the exit of the focusing zone. The geometry was meshed with a body-fitted quadrilateral grid of approx. 30,000 cells. The perturbations imposed on the jet at the inlet were modeled by a time-periodic body force defined inside the first few computational cells downstream from the inlet patch, with a force vector pointing in radial direction. As a result of this force the jet surface is deformed in a sinusoidal manner. In order to allow a meaningful comparison to the semi-analytical results of the foregoing section, it has to be made sure that the perturbations imposed at the inlet dominate over possible numerical fluctuations present in the bulk which, however, might as well induce a decay of the jet. In Fig. 7 simulation results for $\alpha_0/a_0 \approx 0.25$ are displayed, where the same fluid properties as in the previous section were chosen. For comparison, the bottom of the figure shows the jet shape when no perturbations are imposed at all. The inner and the outer liquid are colored in white and gray, respectively. As apparent from the figure, the perturbations grow and their wavelength increases as they are convected away from the inlet. For

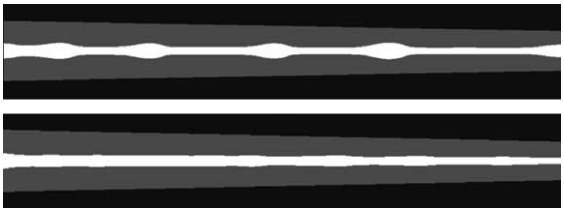

Fig. 7. Shape of a liquid jet on which perturbations have been imposed (above) and the same without perturbations (below).

comparison the jet in the lower part of the figure shows significantly less perturbations of its surface. However, some fluctuations—most likely originating from numerical noise—are visible. Hence, for $\alpha_0/a_0 \approx 0.25$ the imposed perturbations clearly dominate over the numerical ones, a fact which might no longer be true for smaller excitation amplitudes. Another reason not to choose too small perturbation amplitudes is the resolution of the computational grid: When the deflection of the fluid interface is of the same order of magnitude as the lateral extension of the computational cells, it is no longer possible to resolve a perturbation numerically. For this reason, the semi-analytical approach of the previous section and the CFD simulations presented here are in some sense complimentary: While the former is accurate for small perturbation amplitudes, the latter is especially suited for large deflections of the fluid interface.

A time sequence of the fluid distribution for situations where the jet decays within the focusing zone are displayed in Fig. 8. The dynamical evolution of the perturbations is such that already quite close to the inlet the interface shape deviates considerably from that of a focused jet with a sinusoidal excitation. Rather than that, pronounced "bumps" develop which are connected by comparatively thin threads. The position where the jet decays into droplets or fragments undergoes large fluctuations, i.e., in the same simulation the z-positions where a thread ruptures and the jet decays into different parts usually vary. In Fig. 8 the disintegration of the jet in the last frame occurs comparatively close to the inlet. The computational grid was chosen such that in radial direction the geometry is resolved with 28 cells and the radial extension of a cell located at $r = 0$ is about a factor of 40 smaller than the corresponding extension of the focusing zone.

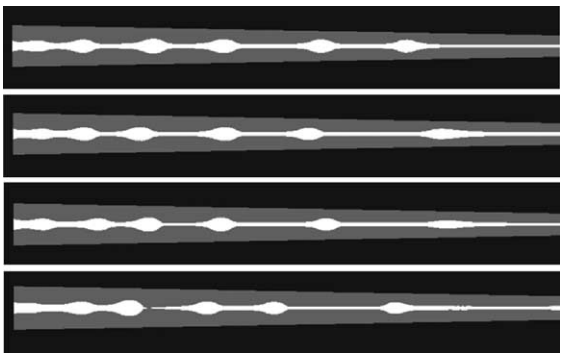

Fig. 8. Time sequence of the shape of an excited liquid jet for a situation where the jet decays into droplets within the focusing zone.

When the flow velocity is increased, the position of jet decay is shifted from the focusing zone to the attached capillary. A corresponding time sequence is displayed in Fig. 9. The thinnest thread visible in the uppermost frame of the figure is still resolved with about four computational cells in radial direction (or, equivalently, eight cells if based on the thread diameter instead of the radius). As indicated from the figure, the decay into droplets proceeds in a more regular manner than in the case of fragments or droplets being formed within the focusing zone. Due to the dominance of viscous over surface tension forces, the droplets assume an elongated shape with sharp cusps at both ends. When comparing the computed jet and droplet shapes to experimental results for the breakup of highly viscous jets, a qualitative agreement is found. Both the "beads-on-a-string" structure in Fig. 8 and the elongated, cusped droplets of Fig. 9 are described in the review article of Eggers (1997).

The CFD method with its ability to model large deformations of the fluid interface and droplet formation is able to describe phenomena well beyond the scope of the semi-analytical approach presented in the previous section. This is demonstrated by the formation of secondary "jets", i.e., thin liquid threads depicted in Fig. 10. The four frames show a droplet which has been created close to the entrance to the focusing zone and is convected downstream while being subjected to the shear forces of the extensional flow. When advancing into the increasingly narrow flow domain the droplet becomes elongated and forms a thin thread when entering the capillary section attached to the focusing zone. Hence, even at comparatively low velocities for which the primary droplet formation occurs close to the inlets, small secondary droplets may be created via breakup of the thread formed within the capillary section. In the CFD simulations presented here the length of the capillary section was too short to observe a decay into droplets. In contrast to the situation where perturbations are imposed at the inlet to the focusing zone, there is no

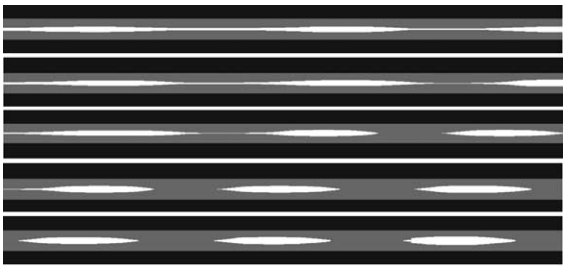

Fig. 9. Time sequence of the shape of an excited liquid jet and the emerging droplets for a situation where the jet decay occurs inside the capillary attached to the focusing zone.

Fig. 10. Time sequence of a droplet having been created close to the entrance of the focusing zone and being stretched by hydrodynamic shear forces while convecting downstream.

straightforward way to control the spectrum of perturbations of the secondary thread. In general one would expect the thread to decay via the fastest growing perturbation mode.

A comparison of the results of the CFD and the semi-analytical model can help to asses the range of validity of the latter and to highlight the reasons for possible deviations. One of the most obvious quantities to be extracted is the decay length of the jet z_d. A comparison of the decay lengths derived from the different models as a function of the inlet velocity is shown in Fig. 11. In the case of the semi-analytical model, the naive definition of the decay length as presented in the previous section was used. The CFD prediction for the decay length was obtained from the position of jet breakup and droplet formation. Only three data points derived from the CFD simulation are shown in the diagram (besides the trivial one at an inlet velocity of zero), however, more could be added at inlet velocities below 7 mm/s where the formation of droplets occurs at the inlet (i.e., the decay length is zero). The dashed line connecting the data points is drawn to guide the eye. For inlet velocities between 8 and 9 mm/s it is very difficult to exactly fix the coordinate of the CFD data points on the y-axis, since the decay within the focusing zone is quite irregular and the z-position of droplet or fragment formation undergoes large fluctuations. However, from a velocity of about 9 mm/s on the breakup of the jet no longer occurs within the focusing zone. This transition is indicated by the data point corresponding to a decay length of $z_d/L = 1$.

The decay length derived from the semi-analytical model, indicated by the solid line in Fig. 11, is smaller than the CFD prediction for most inlet velocities, i.e., the semi-analytical model predicts less stable jets decaying closer to the inlet. The inlet velocity for which a transition to a situation occurs where the jet no longer decays in the focusing zone is about one order of magnitude higher as high as for the CFD simulation. A possible explanation for these deviations can be found when analyzing the velocity field of the outer liquid close to the channel walls, as displayed in Fig. 12. The upper part of the figure shows a jet with perturbations being focused into the converging channel section. The z-component of the flow velocity was evaluated along the dashed line parallel to the upper channel wall and is plotted in the lower part of the figure. The velocity profile exhibits

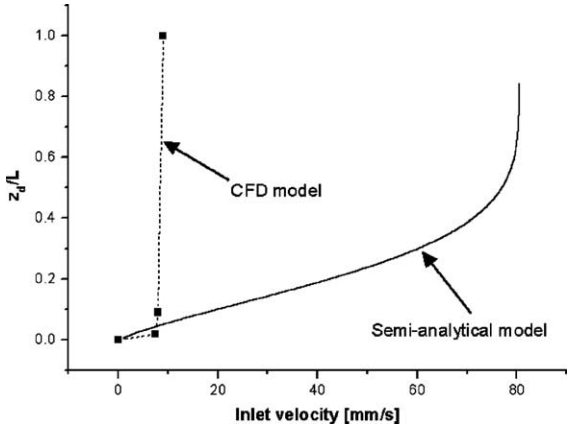

Fig. 11. Jet decay length divided by the extension of the focusing zone as a function of inlet velocity as derived from the semi-analytical and the CFD model.

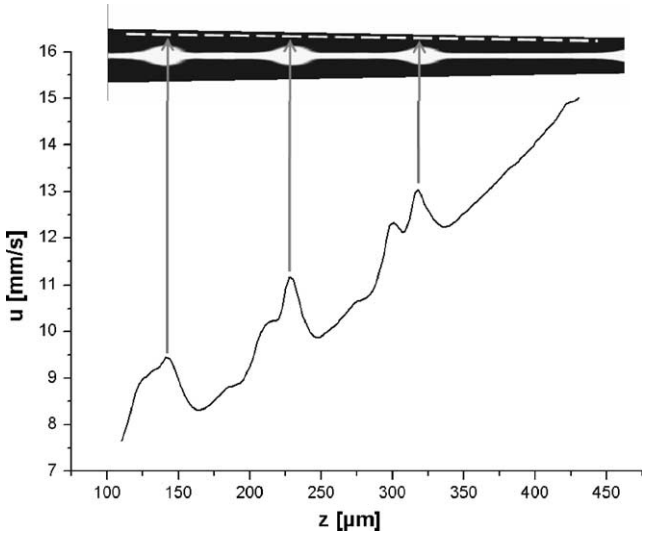

Fig. 12. Velocity profile in the outer liquid close to the channel wall of the focusing section. In the upper part of the figure the corresponding shape of the jet with three distinct bulges is displayed.

three maxima at the positions of the bulges of the jets. These velocity maxima are due to the proximity of the channel walls and exert shear forces onto the bulges which tend to damp their further growth. Hence, in those stages where the bulges of the jet have grown considerably the interaction with the channel walls, mediated by the outer fluid, slows down the further increase of perturbations. The deviations between the CFD and the semi-analytical results are likely to be due to these wall interaction effects, at least in part. Other sources of a modified growth dynamics are nonlinear effects which are not included in the semi-analytical model. Nonlinearities induce a coupling between the different harmonic modes and might as well slow down the growth of perturbations. Fig. 8, exhibiting perturbations which can no longer be described by harmonic functions, shows clear indication of nonlinear dynamics and mode coupling.

4. Summary and conclusions

A semi-analytical and a CFD model have been presented allowing to describe the growth of perturbations on a focused liquid jet. The semi-analytical model relies on the Stokes-flow approximation and is valid for small-amplitude perturbations on a slowly focused liquid jet. In contrast to that, the CFD model is suited to model surface deformations of comparatively large amplitude and even breakup into droplets and is not restricted to small Reynolds numbers. In all of the studies a harmonic perturbation was imposed on the jet at the inlet.

When studying the growth of perturbations with the semi-analytical model, excitations which are subcritical close to the inlet due to their short wavelength may suddenly start to grow at a downstream position owing to the extensional flow related to hydrodynamic focusing and the wavelength scaling going along with that. When approaching the exit of the focusing zone the flow velocity increases rapidly, leading to an apparent slowing down of the growth rate of the perturbations when

represented as a function of the axial coordinate. Depending on the position where the perturbation amplitudes are measured, different modes may be identified as the most unstable ones. When plotting the decay length of the jet as a function of the dimensionless excitation wave number, curves with a quite broad minimum, representing the most unstable mode, are found.

In the corresponding CFD simulations the jets assume a characteristic "beads-on-a-string" shape before decaying into droplets. When the breakup occurs in the capillary section attached to the focusing zone, elongated droplets with cusped ends are formed. Even when comparatively large droplets are created close to the inlet to the flow domain, a secondary liquid thread may emerge when the droplet is elongated by the extensional flow and enters the capillary section. Hence, for a sufficiently long capillary section small droplets may be created by breakup of this secondary thread. The decay length obtained from the CFD results was compared to the corresponding quantity obtained from the semi-analytical results. The jets observed in the CFD simulations were found to be more stable than suggested by the predictions of linear stability theory, with the critical velocity where the jet enters the capillary section reduced by about an order of magnitude. The difference between the CFD and the analytical results was further investigated and it was found that for the geometry considered the jet interacts with the surrounding channel walls. By virtue of this interaction the velocity field of the outer liquid exhibits maxima at the positions of the bulges of the jet. The shear forces due to these velocity maxima should slow down a further growth of the bulges and could explain the discrepancy between the results obtained with the semi-analytical and the CFD model. In addition to that, the CFD model includes nonlinear effects which have been neglected in the semi-analytical model. When attempting to use the semi-analytical model to estimate the instability of a focused jet, care should be taken that the maximum radial extension of the jet is small compared to the radius of the channel.

While "ordinary" cylindrical jets already exhibit very rich dynamics and show different behavior in different fluidic regimes, the phenomena related to the instability of a focused liquid jet are even more diverse. In the present work a focusing zone of conical shape was considered, with a capillary section attached to it as far as the CFD simulation was concerned. More interesting dynamics may be expected when more general flow domain geometries are taken into account. As an example, a focusing section might be followed by a widening channel, leading to a defocusing which may stabilize initially unstable perturbations. Such set ups are waiting to be explored both experimentally and theoretically and may find applications in microfluidic systems such as microreactors.

Acknowledgment

This work was supported in part by grant number HA 2696/2-1 of the Deutsche Forschungsgemeinschaft (DFG).

References

Anna, S.L., Bontoux, N., Stone, H.A., 2003. Formation of dispersions using "flow focusing" in microchannels. Appl. Phys. Lett. 82, 364–366.

Akbar, M.K., Plummer, D.A., Ghiaasiaan, S.M., 2003. On gas–liquid two-phase flow regimes in microchannels. Int. J. Multiphase Flow 29, 855–865.

Ashgriz, N., Mashayek, F., 1995. Temporal analysis of capillary jet breakup. J. Fluid Mech. 291, 163–190.

Brackbill, J.U., Kothe, D.B., Zemach, C., 1992. A continuum method for modeling surface tension. J. Comput. Phys. 100, 335–354.

Brenn, G., Lackermeier, U., 1997. Drop formation from a vibrating orifice generator driven by modulated electrical signals. Phys. Fluids 9, 3658–3669.

Chandrasekhar, S., 1961. Hydrodynamic and Hydromagnetic Stability. Oxford University Press, New York/London.

Cole, R.B. (Ed.), 1997. Electrospray Ionization Mass Spectrometry: Fundamentals, Instrumentation, and Applications. John Wiley, New York.

Dreyfus, R.,Tabeling, P., Willaime, H., 2003. Ordered and disordered patterns in two-phase flows in microchannels. Phys. Rev. Lett. 90, 144505-1–144505-4.

Eggers, J., 1997. Nonlinear dynamics and breakup of free-surface flows. Rev. Mod. Phys. 69, 865–929.

Ferziger, J.H., Perić, M., 2002. Computational Methods for Fluid Dynamics, third ed. Springer, Berlin.

Freitas, S., Walz, A., Merkle, H.P., Gander, B., 2003. Solvent extraction employing a static micromixer: a simple, robust and versatile technology for the microencapsulation of proteins. J. Microencapsulation 20, 67–85.

Gañán-Calvo, A.M., 1998. Generation of steady liquid microthreads and micron-sized monodisperse sprays in gas streams. Phys. Rev. Lett. 80, 285–288.

Hardt, S., Schönfeld, F., Weise, F., Hofmann, C., Ehrfeld, W., 2001. Simulation of droplet formation in micromixers. In: Proceedings of MSM2001, 4th Int. Conf. Modeling and Simulation of Microsystems, Hilton Head Island, SC, March 19–21, 2001, pp. 223–226.

Haverkamp, V., Ehrfeld, W., Gebauer, K., Hessel, V., Löwe, H., Richter, T., Wille, C., 1999. The potential of micromixers for contacting of disperse liquid phases. Fresenius J. Anal. Chem. 364, 617–624.

Hetsroni, G., Mosyak, A., Segal, Z., Pogrebnyak, E., 2003. Two-phase flow patterns in parallel micro-channels. Int. J. Multiphase Flow 29, 341–360.

Kawahara, A., Chung, P.M.-Y., Kawaji, M., 2002. Investigation of two-phase flow pattern, void fraction and pressure drop in a microchannel. Int. J. Multiphase Flow 28, 1411–1435.

Leonard, B.P., 1979. A stable and accurate convection modelling procedure based on quadratic upstream interpolation. Comp. Meth. Appl. Mech. Eng. 19, 59–98.

Lin, S.P., Lian, Z.W., 1990. Mechanisms of the breakup of liquid jets. AIAA J. 28, 120–126.

Mikami, T., Cox, R.G., Mason, S.G., 1975. Breakup of extending liquid threads. Int. J. Multiphase Flow 2, 113–138.

Ormerod, M.G., 1999. Flow Cytometry. Bios Scientific Publishers, Oxfordshire, UK.

Pennemann, H., Löb, P., Hardt, S., Hessel, V., Weise, F., 2004. Flüssig/flüssig Dispergierung im Interdigital-Mikromischer. Chemie Ingenieur Technik 76, 651–659.

Reynolds, O., 1886. On the theory of lubrication and its application to Mr. Beauchamp Tower's experiments, including an experimental determination of the viscosity of olive oil. Philos. Trans. R. Soc. London 177, 157–234.

Sugiura, S., Nakajima, M., Iwamoto, S., Seki, M., 2001. Interfacial tension driven monodispersed droplet formation from microfabricated channel array. Langmuir 17, 5562–5566.

Thorsen, T., Roberts, R.W., Arnold, F.H., Quake, S.R., 2001. Dynamic pattern formation in a vesicle-generating microfluidic device. Phys. Rev. Lett. 86, 4163–4166.

Van Doormal, J.P., Raithby, G.D., 1984. Enhancement of the SIMPLE method for predicting incompressible fluid flows. Numer. Heat Transfer 7, 147–163.

Yeh, J.T., 2001. A VOF-FEM and coupled inkjet simulation. In: Proceedings of ASME FEDSM'01, New Orleans, LA, May 19–June 1, 2001, Paper # FEDSM2001-18182.